Cbfβ deletion in mice recapitulates cleidocranial dysplasia and reveals multiple functions of Cbfβ required for skeletal development

Wei Chen[a,1,2], Junqing Ma[a,b,1], Guochun Zhu[a], Joel Jules[a], Mengrui Wu[a,c], Matthew McConnell[a], Fei Tian[a], Christie Paulson[a], Xuedong Zhou[d], Lin Wang[b], and Yi-Ping Li[a,2]

[a]Department of Pathology, University of Alabama at Birmingham, Birmingham, AL 35294; [b]College of Stomatology, Nanjing Medical University, Nanjing 210029, People's Republic of China; [c]Institute of Genetics, Life Science College, Zhejiang University, Hangzhou, Zhejiang 310058, People's Republic of China; and [d]The State Key Laboratory of Oral Diseases, West China College of Stomatology, Sichuan University, Chengdu, Sichuan 610041, People's Republic of China

Edited* by Maria I. New, Icahn School of Medicine at Mount Sinai, New York, NY, and approved January 6, 2014 (received for review June 11, 2013)

The pathogenesis of cleidocranial dysplasia (CCD) as well as the specific role of core binding factor β (Cbfβ) and the Runt-related transcription factor (RUNX)/Cbfβ complex in postnatal skeletogenesis remain unclear. We demonstrate that Cbfβ ablation in osteoblast precursors, differentiating chondrocytes, osteoblasts, and odontoblasts via *Osterix*-Cre, results in severe craniofacial dysplasia, skeletal dysplasia, abnormal teeth, and a phenotype recapitulating the clinical features of CCD. *Cbfβ$^{f/f}$Osterix-Cre* mice have fewer proliferative and hypertrophic chondrocytes, fewer osteoblasts, and almost absent trabecular bone, indicating that Cbfβ may maintain trabecular bone formation through its function in hypertrophic chondrocytes and osteoblasts. *Cbfβ$^{f/f}$Collagen, type 1, alpha 1* (*Col1α1*)*–Cre* mice show decreased bone mineralization and skeletal deformities, but no radical deformities in teeth, mandibles, or cartilage, indicating that osteoblast lineage-specific ablation of Cbfβ results in milder bone defects and less resemblance to CCD. Activating transcription factor 4 (Atf4) and Osterix protein levels in both mutant mice are dramatically reduced. ChIP assays show that Cbfβ directly associates with the promoter regions of *Atf4* and *Osterix*. Our data further demonstrate that Cbfβ highly up-regulates the expression of *Atf4* at the transcriptional regulation level. Overall, our genetic dissection approach revealed that Cbfβ plays an indispensable role in postnatal skeletal development and homeostasis in various skeletal cell types, at least partially by up-regulating the expression of *Atf4* and *Osterix*. It also revealed that CCD may result from functional defects of the Runx2/Cbfβ heterodimeric complex in various skeletal cells. These insights into the role of Cbfβ in postnatal skeletogenesis and CCD pathogenesis may assist in the development of new therapies for CCD and osteoporosis.

osteoblast differentiation | chondrocyte differentiation | ossification | growth plate formation | endochondral bone formation

Core binding factor (Cbf) plays crucial roles during skeletal development and hematopoiesis. Cbf consists of two subunits: Cbf alpha (Cbfα) and Cbf beta (Cbfβ). Runt-related transcription factor 2 (Runx2) has been shown to be critical for the differentiation of osteoblasts and skeletal development. Cleidocranial dysplasia (CCD) mainly stems from *Runx2* deficiency and is characterized by hypoplastic/aplastic clavicles, patent fontanelles, supernumerary teeth, and short stature (1–3). Notably, there were two case reports of CCD patients with no *RUNX2* mutation involving 16q22 large deletions, suggesting CBFβ haploinsufficiency might be involved in cranial facial defects (4, 5). Although great progress has been made toward understanding the function of Runx2 and Cbfβ during the past 20 y, their function in postnatal skeletogenesis and in the pathogenesis of related diseases (e.g., CCD) still remains unclear.

Runx2-I/*Cbfβ* and *Runx2-II*/*Cbfβ* double transgenic mice had enhanced inhibition of osteoblast maturation, resulting in severe osteopenia and fragility in adult mice (6). There is a lack of genetic evidence establishing a specific effect of the missing Runx2/Cbfβ complex in postnatal skeletogenesis and the pathogenesis of CCD due to the fact that *Runx2*$^{-/-}$ mice die at birth and *Cbfβ*$^{-/-}$ mice die at midgestation (7, 8) and *Cbfβ*$^{GFP/GFP}$ knock-in mice and transgenic rescued *Runx2*$^{-/-}$ mice [*Cbfβ*$^{-/-}$ Tg(*Tek*-GFP/*Cbfb* mice and *Cbfβ*$^{-/-}$ Tg(*Gata1*/*Cbfb*) mice] die soon after birth (9–11). To investigate the role of Cbfβ in postnatal skeletal development and the pathogenesis of CCD, we used *Osterix*-Cre (*Osx*-Cre) mice, which specifically delete *Cbfβ* flanked by *loxP* (*Cbfβ$^{f/f}$*) in osteoblast precursors, differentiating chondrocytes, osteoblasts, and odontoblasts (12, 13), and *Col1α1-Cre* mice, which specifically delete *Cbfβ* in the osteoblast lineage (14). In this study, through the powerful approach of conditional knockout (cKO) for genetic dissection, we are able to provide unique insight into the pathogenesis of CCD and reveal multiple functions of Cbfβ required for skeletal development.

Results

***Cbfβ$^{f/f}$Osx-Cre* Mice Have Decreased Ossification and Skeletal Deformities, Resulting in a CCD-Like Phenotype.** *Cbfβ$^{f/f}$Osx-Cre* mice survived into adulthood, but the homozygote mice displayed severe postnatal skeletal defects. Three-wk-old *Cbfβ$^{f/f}$Osx-Cre* mice were of a dispoportionately short stature compared with their wild-type (WT) cohorts (Fig. 1*A*). X-ray analysis of femurs from 3-wk-old *Cbfβ$^{f/f}$Osx-Cre* mice showed decreased growth and

Significance

Cleidocranial dysplasia (CCD) is a hereditary human skeletal disease. Mutations in *Runt-related transcription factor 2*, which functions as a heterodimer with core binding factor β (Cbfβ), are found in most individuals with CCD. It has been suspected that Cbfβ may be responsible for other CCD cases. The pathogenesis of CCD and the role of Cbfβ in postnatal skeletogenesis remain unclear. There has been no animal model to study this disease. We demonstrate that ablation of Cbfβ in various skeletal cells results in severe craniofacial and skeletal dysplasia with the phenotype recapitulating clinical features of CCD. The findings from this study of Cbfβ in the skeleton provide insight into the role of Cbfβ in postnatal skeletogenesis and pathogenesis of CCD, which may assist in developing new therapies for CCD and osteoporosis.

Author contributions: W.C. and Y.-P.L. designed research; W.C., J.M., G.Z., and F.T. performed research; W.C., J.M., G.Z., J.J., M.W., M.M., F.T., C.P., X.Z., L.W., and Y.-P.L. analyzed data; and W.C., J.J., C.P., and Y.-P.L. wrote the paper.

The authors declare no conflict of interest.

*This Direct Submission article had a prearranged editor.

[1]W.C. and J.M. contributed equally to this work.

[2]To whom correspondence may be addressed. E-mail: ypli@uab.edu or wechen@uab.edu.

This article contains supporting information online at www.pnas.org/lookup/suppl/doi:10.1073/pnas.1310617111/-/DCSupplemental.

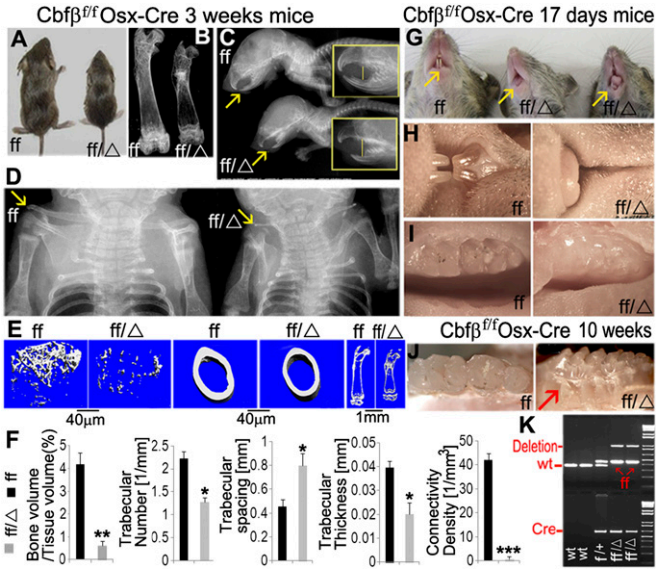

Fig. 1. *Cbfβ$^{f/f}$ Osx-Cre* mice have decreased bone mineralization and skeletal deformities, resulting in a CCD-like phenotype. (*A*) Photographic analysis of 3-wk-old *Cbfβ$^{f/f}$ Osx-Cre* (ff/Δ) mice and WT (ff) mice. (*B–D*) X-ray analysis of (*B*) femurs, (*C*) mandibles, and (*D*) clavicles. Yellow arrows in *C* and *D* indicate that *Cbfβ$^{f/f}$ Osx-Cre* mice have a severe anterior open bite and mandibular retrognathism as well as hypoplastic/aplastic clavicles, respectively. (*E* and *F*) The μCT scans (*E*) and quantification (*F*) show that bones from *Cbfβ$^{f/f}$ Osx-Cre* mice are smaller and less mineralized than those of WT. (*G* and *H*) Photographic analysis (*G*) and high magnification (*H*) of incisor tooth development. Yellow arrows indicate normal (left mouse), stunted (middle mouse), or abnormal (right mouse) tooth development. (*I*) High-magnification analysis of molar tooth development. (*J*) Photographic analysis shows defective, supernumerary-like teeth (red arrow) in *Cbfβ$^{f/f}$ Osx-Cre* mice compared with WT. (*K*) All mice were genotyped by PCR from tail snip DNA.

reduced ossification (Fig. 1*B*). *Cbfβ$^{f/f}$Osx-Cre* mice also exhibited underdeveloped mandibles and mandibular retrognathism, resulting in a large gap inside the oral cavity and causing an anterior open bite, and severely affected teeth (Fig. 1*C*). X-ray analysis revealed hypoplasia/aplasia of clavicles and underdeveloped long bones, leading to severe deformities in the mutant mice (Fig. 1*D*). These skeletal defects persisted in 3- and 10-wk-old *Cbfβ$^{f/f}$ Osx-Cre* mice (Fig. S1). Classical CCD is caused by RUNX2 haploinsufficiency. Our results showed that there was a milder CCD phenotype in *Cbfβ* cKO heterozygous mice and a more severe CCD phenotype in *Cbfβ* cKO homozygous mice (Fig. S1*E*). Microcomputed tomography (μCT) scan of femurs revealed a drastic decrease in bone density and an almost complete lack of trabecular bone in the mutant mice (Fig. 1 *E* and *F*). Moreover, incisors were completely absent (Fig. 1*G*, middle mouse) or severely underdeveloped in 17-d-old *Cbfβ$^{f/f}$ Osx-Cre* mice (Fig. 1*G*, right mouse). Higher magnification further illustrated the underdeveloped incisors (Fig. 1*H*) and underdeveloped molars in *Cbfβ$^{f/f}$Osx-Cre* mice (Fig. 1*I*). The teeth defects were still apparent in 10-wk old mutant mice, which also exhibited a supernumerary teeth-like phenotype, a clinical feature of CCD (Fig. 1*J*). The genotypes of the mice were confirmed by PCR (Fig. 1*K*) from tail snip DNA. These results showed that Cbfβ ablation in osteoblast precursors results in many clinical features of CCD, including short stature, hypoplastic/aplastic clavicles, and dental anomalies.

***Cbfβ$^{f/f}$Osx-Cre* Mice Have Shortened Limbs, Decreased Bone Ossification, and Disproportionately Defective Skull, Calveria, and Mandible.** Alizarin red and Alcian blue staining showed that, except for the vertebrae and sternum, every bone in 6-d-old *Cbfβ$^{f/f}$Osx-Cre* mice was severely underdeveloped (Fig. 2*A*). However, some bones showed greater defects than other bones. The skull, calveria, and mandible were not only undercalcified in the mutant mice, but also displayed patent fontanelles (Fig. 2*B*). Moreover, the forelimbs (Fig. 2*C*) and clavicles (Fig. 2*D*) were severely affected in the mutant mice, whereas, again, the vertebrae were largely unaffected (Fig. 2*E*). The mandibula, hyoid bone, thyroid cartilage, and cricoid cartilage in the newborn *Cbfβ$^{f/f}$Osx-Cre* mice were also underdeveloped due to decreased ossification (Fig. S2). Further, the underdevelopment of the hyoid bone was still apparent in 6-d-old *Cbfβ$^{f/f}$Osx-Cre* mice. Overall, the skeleton of the mutant mice was severely underdeveloped compared with normal littermates. The data suggest that the process of bone ossification was delayed in mutant mice. Notably, *Cbfβ$^{f/f}$Osx-Cre* mice had patent fontanelles, another common characteristic of CCD.

***Cbfβ$^{f/f}$Osx-Cre* Newborn Tibiae Have Impaired Endochondral and Intramembranous Bone Ossification, and Goldner's Trichrome Staining Revealed a Decrease in Osteoblasts Numbers Through Histomorphometric Analysis.** To further analyze the growth retardation observed in the *Cbfβ$^{f/f}$Osx-Cre* mice, we performed hematoxylin/eosin (H&E), Von Kossa, Alcian blue, and Safranin O staining on tibia from newborn mice. Newborn *Cbfβ$^{f/f}$Osx-Cre* mice had decreased ossification and endochondral bone formation (Fig. 3 *A* and *B*). Newborn *Cbfβ$^{f/f}$Osx-Cre* mice had decreased cartilage and underdeveloped growth zones, which may partially stem from the reduction in chondrocytes of the hypertrophic region of the growth plate in mutant mice (Fig. 3 *A–C*). Furthermore, we found that the columns of proliferating and hypertrophic chondrocytes were less organized in *Cbfβ$^{f/f}$Osx-Cre* mice (Fig. 3*C*). We also found a decrease in intramembranous bone formation in *Cbfβ$^{f/f}$Osx-Cre* mice as assessed by H&E staining (Fig. 3*D*). Finally, Von Kossa and Fast red staining revealed a substantial decrease in calcium and a significantly shorter medullary cavity in 10-wk-old *Cbfβ$^{f/f}$Osx-Cre* mice compared with control mice (Fig. 3*E*). Collectively, these results demonstrate that *Cbfβ$^{f/f}$Osx-Cre* mice survive to adulthood and recapitulate the clinical features of CCD. Goldner's Trichrome

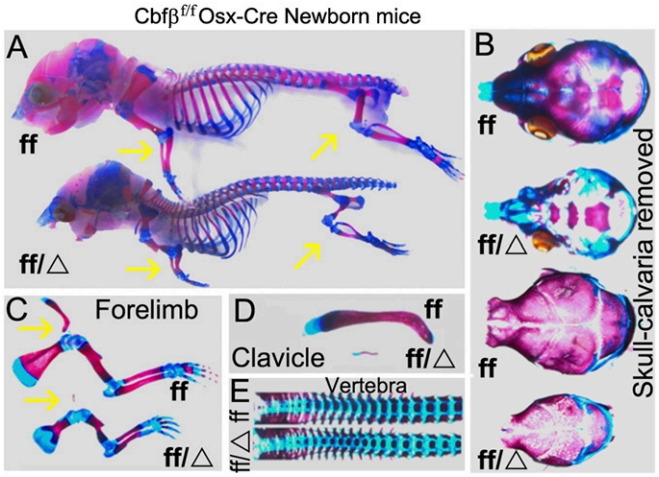

Fig. 2. *Cbfβ$^{f/f}$ Osx-Cre* mice have shortened limbs, decreased bone ossification, and disproportionately defective skull, calveria, and mandible. (*A*) Whole-mount skeletal was stained by Alizarin red and Alcian blue staining of newborn *Cbfβ$^{f/f}$ Osx-Cre* (ff/Δ) and WT (ff) mice. Yellow arrows show reduced bone ossification in the limbs of the mutant mice. (*B–E*) The skull (*B*), forelimbs (*C*), clavicles (*D*), and vertebrae (*E*) of the mutant mice display decreased ossification. Yellow arrows in *C* show that the mutant mice have less calcified trabecular bone adjacent to the hypertrophic zone.

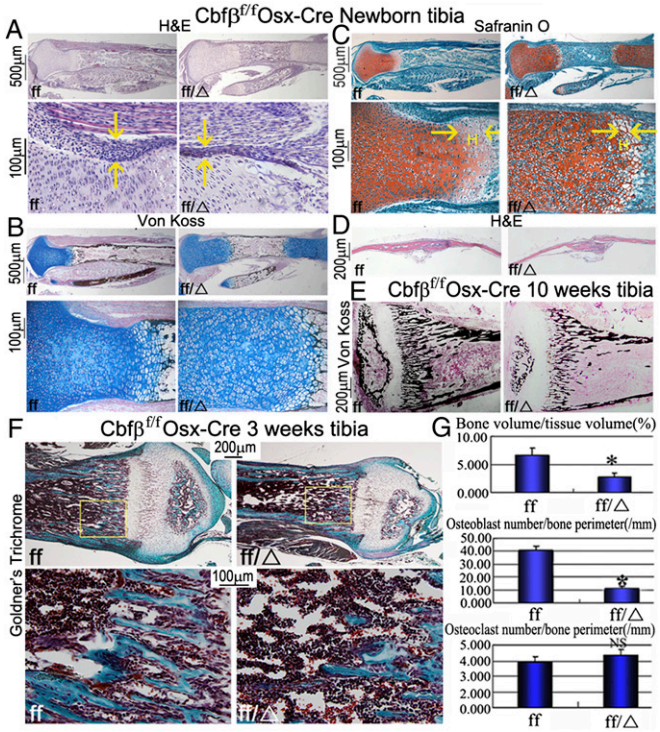

Fig. 3. *Cbfβ*$^{f/f}$*Osx-Cre* newborn tibiae have impaired endochondral bone ossification, and Goldner's Trichrome staining revealed a decrease in osteoblast numbers. (*A*–*C*) H&E staining (*A*), Von Kossa and Alcian blue staining (*B*), and Safranin O staining (*C*) of tibiae from newborn *Cbfβ*$^{f/f}$ *Osx-Cre* (ff/Δ) and WT (ff) mice. Yellow arrows in *A* and *C* indicate that *Cbfβ*$^{f/f}$ *Osx-Cre* mice have a reduced bone collar and fewer hypertrophic chondrocytes in the growth plate, respectively. (*D*) H&E staining shows defective intramembranous bone formation in newborn mutant mice compared with WT. (*E*) Von Kossa staining of tibia from 10-wk-old *Cbfβ*$^{f/f}$ *Osx-Cre* and WT bones. (*F*) Goldner's Trichrome stain of hard-tissue sections of tibia from 3-wk-old *Cbfβ*$^{f/f}$ *Osx-Cre* (ff/Δ) and WT (ff) mice. For histological detail of trabeculae, the bottom row shows a higher magnification of areas in yellow boxes. (*G*) Quantification of the data shown in *F*.

staining revealed a decrease in bone density in *Cbfβ*$^{f/f}$*Osx-Cre* (Fig. 3*F*) and *Cbfβ*$^{f/f}$*Col1α1-Cre* mice (Fig. S3*B*). Notably, there was a significant decrease in bone volume and fewer osteoblasts in the *Cbfβ*$^{f/f}$*Osx-Cre* mice (Fig. 3*G*), but the number of osteoclasts was not significantly affected (Fig. 3*G*). The tartrate-resistant acid phosphatase staining confirmed that the number of osteoclasts was not significantly affected in *Cbfβ*$^{f/f}$*Osx-Cre* mice (Fig. S3*A*). Goldner's Trichrome staining also showed that there was a significant decrease in bone volume and fewer osteoblasts (Fig. S3*B*), but the number of osteoclasts was not significantly affected in *Cbfβ*$^{f/f}$*Col1α1-Cre* tibia sections (Fig. S3 *B* and *C*).

***Cbfβ*$^{f/f}$*Col1α1-Cre* Mice Have Decreased Bone Mineralization and Skeletal Deformities but No Radical Deformities in Teeth, Mandibles, or Cartilage.** Because *Cbfβ*$^{f/f}$*Osx-Cre* mice delete the *Cbfβ* gene in both osteoblasts and hypertrophic chondrocytes, we generated *Cbfβ*$^{f/f}$*Col1α1-Cre* mice to observe the impact of Cbfβ specifically in the osteoblast lineage during postnatal bone development (Fig. 4). Similar to the *Cbfβ*$^{f/f}$*Osx-Cre* mice (Fig. 1), bone formation was severely inhibited in *Cbfβ*$^{f/f}$*Col1α1-Cre* mice, leading to shorter stature and decreased bone density compared with WT mice (Fig. 4 *A*–*C*). Unlike *Cbfβ*$^{f/f}$*Osx-cre* mice (Fig. 1), the clavicle (Fig. 4*B*), mandibles and teeth (Fig. 4*D*), and intramembranous bone formation (Fig. 4*E*) were not dramatically affected in *Cbfβ*$^{f/f}$*Col1α1-Cre* mice. Safranin O staining revealed that there is a shortened growth plate, a decreased and disorganized proliferative zone, and a lack of hypertrophic chondrocytes in *Cbfβ*$^{f/f}$ *Osx-Cre* mutant mice (Fig. 4*F*). However, the growth plate development in *Cbfβ*$^{f/f}$ *Col1α1-Cre* mutant mice is normal compared with the WT mice control (Fig. 4*G*).

***Cbfβ* Deficiency Affects Chondrocyte Proliferation and Maturation in *Cbfβ*$^{f/f}$*Osx-Cre* Mice.** Further examination of the impact of the *Cbfβ* deletion in chondrocytes through proliferating cell nuclear antigen (PCNA) staining revealed that there is a reduction in proliferative chondrocytes in both the resting and proliferation zones of the *Cbfβ*$^{f/f}$*Osx-Cre* but not in the *Cbfβ*$^{f/f}$*Col1α1-Cre* mice (Fig. 5*A*). This is due to the fact that *Cbfβ*$^{f/f}$ *Osx-Cre* mice excise the *Cbfβ* gene in odontoblasts, osteoblasts, and chondrocytes, whereas *Cbfβ*$^{f/f}$*Col1α1-Cre* mice only delete *Cbfβ* in the osteoblast lineage. Importantly, this finding indicates that *Cbfβ* is required for chondrocyte differentiation and the subsequent

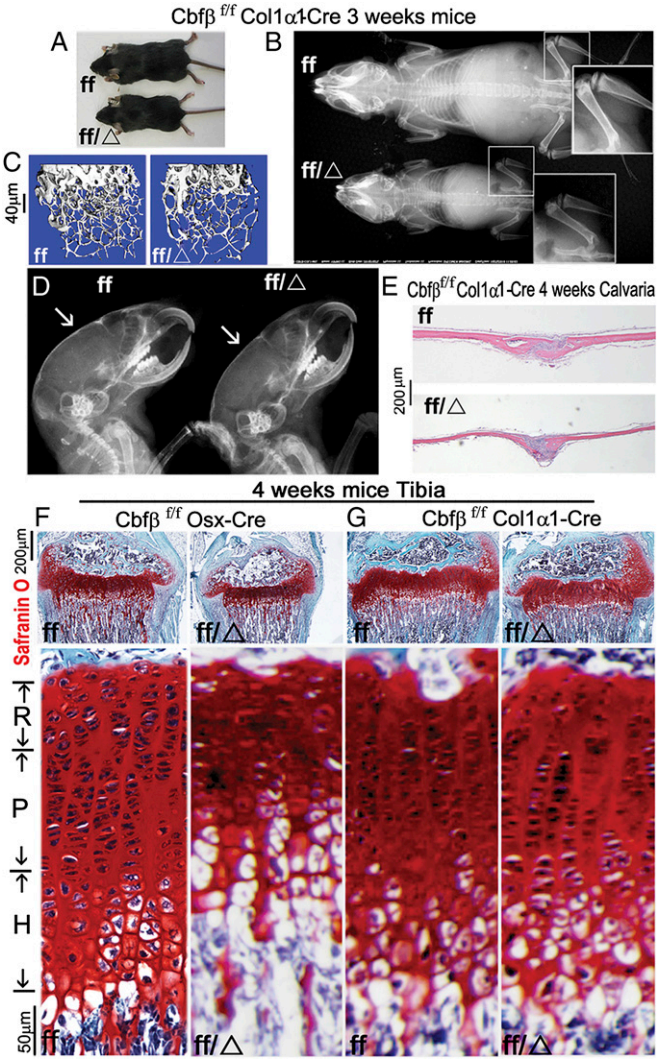

Fig. 4. *Cbfβ*$^{f/f}$*Col1α1-Cre* mice have decreased bone mineralization and skeletal deformities, but no radical deformities in teeth, mandibles, or cartilage. (*A*–*D*) Photographic analysis (*A*), X-ray analysis focusing on femoral bone density (*B*), μCT scans of femurs (*C*), and X-ray analysis of calvaria (*D*) of 3-wk-old *Cbfβ*$^{f/f}$ *Col1α1-Cre* (ff/Δ) and WT (ff) mice. White arrows in *D* show that the calvaria are less calcified in the mutant mice. (*E*) H&E staining shows that intramembranous bone formation was not dramatically affected in *Cbfβ*$^{f/f}$*Col1α1-Cre* mice compared with WT. (*F* and *G*) Safranin O staining of tibia and comparison of growth plate development among 4-wk-old *Cbfβ*$^{f/f}$ *Osx-Cre* mutant, *Cbfβ*$^{f/f}$*Col1α1-Cre* mutant, and WT mice.

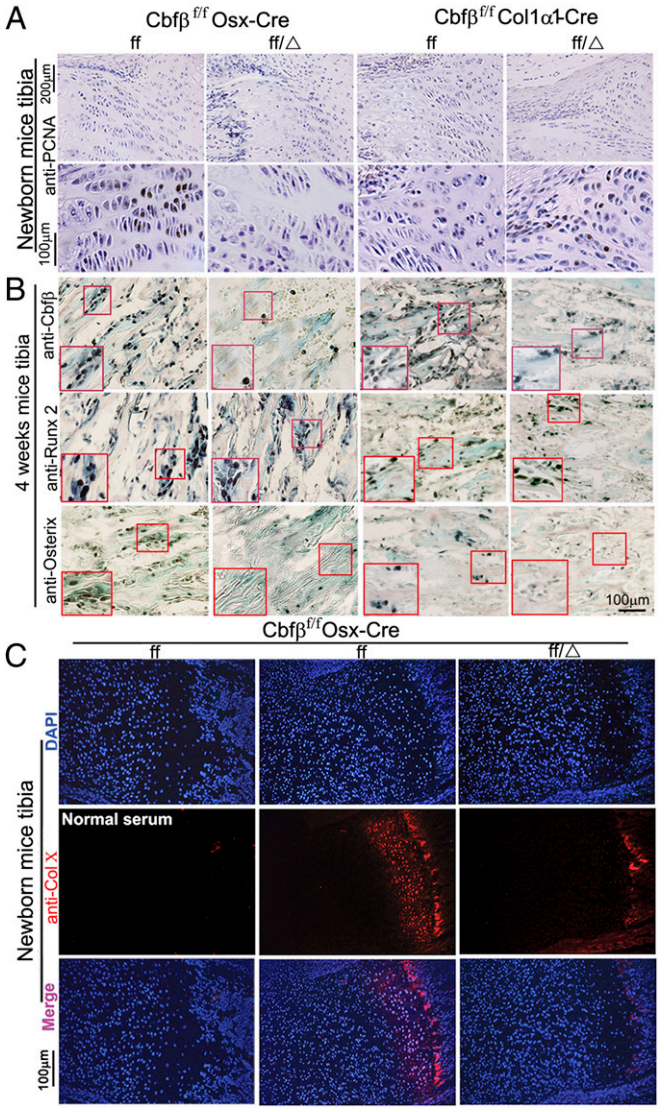

Fig. 5. *Cbfβ* deficiency decreases chondrocyte proliferation, reduces expression of Cbfβ and Osterix, and impairs chondrocyte hypertrophy in *Cbfβ*$^{f/f}$ *Osx-Cre* mice. (*A* and *B*) PCNA staining for cellular proliferation (*A*) and immunohistochemistry (IHC) staining with anti-Cbfβ, anti-Runx2, and anti-osterix antibodies (*B*) of tibial paraffin sections from 4-wk-old *Cbfβ*$^{f/f}$ *Osx-Cre* (ff/Δ), *CbfβfIf Col1α1-Cre* (ff/Δ), and WT (ff) mice. (*Insets*) The magnified images of the red boxed areas, which show a decrease in chondrocyte proliferation in *Cbfβ*$^{f/f}$ *Osx-Cre* mice and reduced expression of Cbfβ and Osterix in both mutant mice compared with WT. (*C*) Immunofluorescence staining of the tibia from newborn *Cbfβ*$^{f/f}$ *Osx-Cre* (ff/Δ) and WT (ff) mice.

growth plate formation during postnatal skeletal development. As several studies indicate that Cbfβ interacts with Runx1, Runx2, and Runx3 during skeletal development, we examined whether the Cbfβ deficiency affected the expression of Runx1, Runx2, and Runx3. Immunohistochemistry analysis showed that there is a reduction in the expression of Osx and Cbfβ in *Cbfβ*$^{f/f}$*Osx-Cre* and *Cbfβ*$^{f/f}$ *Col1α1-Cre* mice but that *Cbfβ* deletion did not affect the level of Runx2 expression (Fig. 5*B*). Immunostaining analysis of newborn *Cbfβ*$^{f/f}$*Osx-Cre* and WT mice femur showed that Runx1 expression was mainly detected in the proliferative zone, Runx2 expression was mainly detected in the hypertrophic zone, and Runx3 expression was mainly detected in hypertrophic and prehypertrophic chondrocytes (Fig. S4 *A–C*). Interestingly, expression of Runx1, Runx2, and Runx 3 showed no variation between WT and mutant mice (Fig. S4 *A–C*). Immunostaining analysis of newborn mice showed a drastic reduction in the expression of Collagen X (ColX), which is a marker of hypertrophic chondrocytes, in the growth plates of *Cbfβ*$^{f/f}$*Osx-Cre* mice (Fig. 5*C*). These results demonstrate that chondrocyte proliferation and maturation are dependent on Cbfβ's function.

***Cbfβ* Deficiency in Primary Calvarial Cells Cultured from *Cbfβ*$^{f/f}$ *Osx-Cre* and *Cbfβ*$^{f/f}$*Col1α1-Cre* Mice Inhibits Osteoblastogenesis.** We investigated the impact of *Cbfβ* deletion on osteoblastogenesis. Calvarial cells from *Cbfβ*$^{f/f}$*Osx-Cre* (Fig. 6*A*) and *Cbfβ*$^{f/f}$*Col1α1-Cre* mice (Fig. S5*A*) after 14 d of culture showed reduced alkaline phosphatase (ALP), indicating a decreased number of osteoblasts in the mutant cells. The reduction in mineralization observed in *Cbfβ*$^{f/f}$*Osx-Cre* was characterized by Von Kossa staining after 21 d of culture (Fig. 6*A*). GeneChip analysis indicated that *Atf4* mRNA expression in mouse C57/BL6 WT calvarial cells on day 7 and day 21 of osteoblastogenesis is similar to that of *secreted phosphoprotein 1* (*Spp1*), *ALP liver/bone/kidney* (*Alpl*), and *Col1α1*, whereas *osteocalcin* (*OCN*) has mRNA expression levels that were much higher (Fig. 6*B*). Further microarray data analysis revealed that *Atf4* mRNA expression in mouse calvarial cells increased more than 10-fold on culture day 21 (Fig. 6*B*). The dramatic changes in *Atf4* mRNA expression were confirmed by quantitative RT-PCR using *Cbfβ*$^{f/f}$*Osx-Cre*, *Cbfβ*$^{f/f}$*Col1α1-Cre*, and WT mouse calvarial cells during osteoblastogenesis (Fig. 6*C*, Fig. S5 *B* and *C*, and Fig. S6). Western blot was used

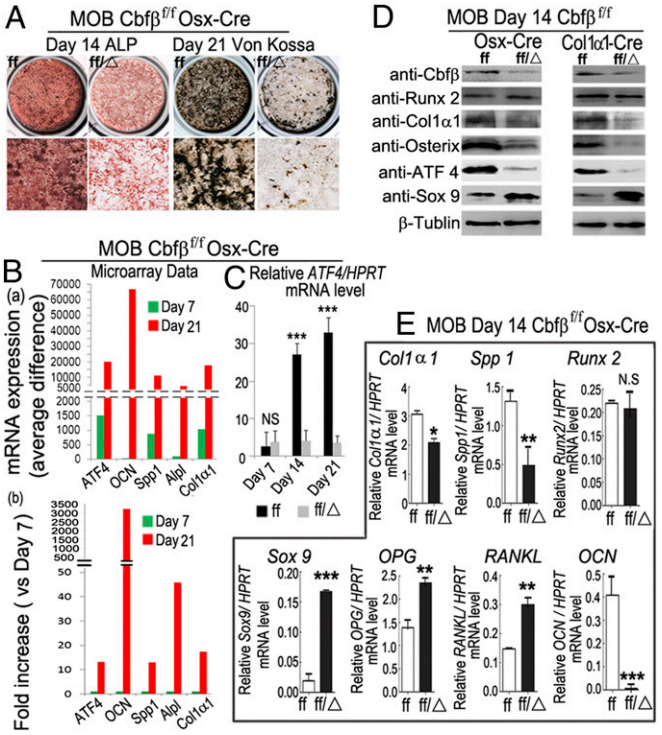

Fig. 6. *Cbfβ* deficiency in primary calvarial cells cultured from *Cbfβ*$^{f/f}$*Osx-Cre* and *Cbfβ*$^{f/f}$*Col1α1-Cre* mice inhibits osteoblastogenesis. (*A*) Calvarial cells from *Cbfβ*$^{f/f}$ *Osx-Cre* (ff/Δ) and WT (ff) newborn mice were applied to osteoblastogenesis assays. (*B*) GeneChip analysis of the expression of *Atf4*, *Ocn*, *Spp1*, *Alpl*, and *Col1α1* in mouse calvarial cells. (*C*) qPCR analysis of the mRNA expression level of *Atf4* in mouse calvarial cells after culturing in the osteoblast differentiation media. (*D*) Protein expression levels were analyzed by Western blot analysis. (*E*) qPCR analysis of mRNA expression levels of *Col1α1*, *Spp1*, *Runx2*, *Sox9*, *OPG*, *RANKL*, and *OCN* in calvaria-derived osteoblasts from *Cbfβ*$^{f/f}$ *Osx-Cre* (ff/Δ) and WT (ff) mice. Results are expressed as mean ± SD, $n \geq 6$ in each group. $^{*}P < 0.05$, $^{**}P < 0.01$, $^{***}P < 0.005$.

to analyze the expression of several key factors that influence osteoblast functions in *Cbfβ*$^{f/f}$*Osx-Cre* and *Cbfβ*$^{f/f}$*Col1α1-Cre* mice. *Cbfβ* deficiency reduced the expression of Cbfβ, Osx, Col1α1, and Atf4, but not Runx2 (Fig. 6*D*). In contrast, the expression of *SRY* (*sex determining region Y*)*-box 9* (*Sox9*) was increased in *Cbfβ*-deficient calvaria-derived osteoblasts (Fig. 6*D*). Taken together, these results demonstrate that Cbfβ deletion impacts chondrocyte and osteoblast differentiation by affecting the expression of critical downstream genes at the mRNA level. Notably, on day 14, *Cbfβ*$^{f/f}$*Osx-Cre* calvarial cells still expressed some *Col1α1* and *Spp1* but not *OCN* (Fig. 6*E*). These data indicate that osteoblasts generated from *Cbfβ*$^{f/f}$*Osx-Cre* mice were maintained in an immature stage and prevented from differentiation into mature osteoblasts, which are critical for bone formation.

Cbfβ Up-Regulates *Osterix* and *Atf4* Expression Directly by Associating with Their Promoters. To determine if the Runx/Cbfβ complex binds to *Osx*, *Runx2*, and *Atf4* promoters, chromatin immunoprecipitation (ChIP) assay was performed. We analyzed the respective promoter regions and designed primers accordingly. We found several Runx binding sites in the *Osx* promoter region (–3000/+80), *Runx2* promoter region (–3000/+80), and *Atf4* promoter region (–4000/+80) (Fig. S7). ChIP analysis was performed using the anti-Cbfβ antibody, and the DNA was pulled down, amplified, and analyzed using primers as shown in Fig. S7. The ChIP input value using each primer represents the binding efficiency of an adjacent region around the location of the primer pair. We found that *Osx* primer 4b resulted in the highest value, indicating that Runx binding sites 13–15 in the *Osx* promoter region should be the most efficient (Fig. 7*A*). In addition, *Runx2* primer 4a showed that Runx binding sites 9 and 10 in the *Runx2* promoter region may be most efficient, whereas *Atf4* primer 3a showed that Runx binding site 5 in the *Atf4* promoter region may be the most efficient (Fig. 7 *B* and *C*). The promoter luciferase assay showed that luciferase activity driven by *Atf4* promoters is very low in the absence of Cbfβ (Fig. S8). Luciferase activity was highest when driven by the longest *Atf4* promoter fragment (–4051/+80) and less high when driven by the *Atf4* promoter fragments (–3109/+80 and –1676/+80) in WT cells, but not in the mutant cells. Interestingly, about 70% of the full Luciferase activity driven by the longest *Atf4* promoter fragment (–4051/+80) still remains with the *Atf4* promoter fragment (–500/+80) in WT cells, but not in the mutant cells. This indicates that the *Atf4* promoter region (–500/+80) containing Runx binding sites 5–7 is critical for Cbfβ regulation of *Atf4* gene expression (Figs. S7 and S8). Consistently, the primer 3a amplifying regions near Runx binding sites 5–7 in the *Atf4* promoter gave out the highest value in ChIP assays (Fig. 7*C*), indicating that the Cbfβ/RUNX complex may bind Runx binding sites 5–7 to up-regulate *Atf4* gene expression. There was also a decrease in luciferase expression driven by the *Runx2* promoter (–1580/+80 and –900/+80) in the absence of Cbfβ. However, Runx2 expression does not vary between WT and mutant cells (Fig. 7*D* and Fig. S6*A*). This indicates that there may be some other mechanism driving the steady expression of Runx2 in Cbfβ knockout mice and cells, probably working on a distant end of the *Runx2* promoter (before –1580). In conclusion, we believe that Cbfβ directly associates with the *Osx* and *Atf4* promoter regions and regulates their expression. To confirm these Western and real-time RT-PCR results in calvarial culture experiments, we used protein directly isolated from calvaria (Fig. 7*D* and Fig. S6). The Western blot result is consistent with that from the calvarial culture experiment result (Fig. 6*D* and Fig. 7*D*).

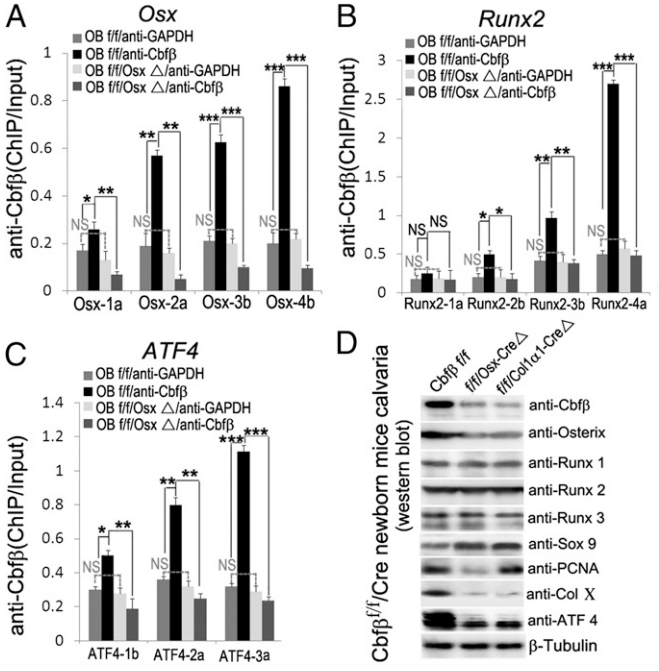

Fig. 7. Cbfβ regulates *Osx*, *Runx2*, and *Atf4* expression by directly associating with their promoters. (*A*–*C*) ChIP analysis of Cbfβ binding to the (*A*) *Osx* promoter, (*B*) *Runx2* promoter, and (*C*) *Atf4* promoter in calvaria-derived osteoblasts using primers as indicated on the *x* axes. Results are presented as ChIP/Input. Results are presented as mean ± SD, $n \geq 6$ in each group. *$P < 0.05$, **$P < 0.01$, ***$P < 0.005$. (*D*) Western blot analysis of the expression of Cbfβ, Osx, Runx1, Runx2, Runx3, Sox9, PCNA, ColX, and Atf4 in the calvaria of newborn *Cbfβ*$^{f/f}$*Osx-Cre*, *Cbfβ*$^{f/f}$*Col1α1-Cre*, and WT mice. β-tubulin is used as the loading control.

Discussion

CCD May Result from a Functional Defect of the Runx2/Cbfβ Heterodimeric Complex in Various Cell Types. Our data show that *Cbfβ*$^{f/f}$*Osx-Cre* mice provide a unique CCD model recapitulating most of the characteristics of human CCD (i.e., wide/open fontanels, midface retrusion, abnormal dentition, severe clavicular hypoplasia, and hand/paw abnormalities). The CCD phenotype of *Cbfβ*$^{f/f}$*Osx-Cre* mice indicates that multiple functions of Cbfβ are required for skeletal development and homeostasis in postnatal skeletogenesis. The fact that the Runx2 protein level was not changed in *Cbfβ*$^{f/f}$*Osx-Cre* cKO mice and that *Cbfβ*$^{f/f}$*Osx-Cre* mice exhibit a CCD-like phenotype (Fig. 1) supports the notion that CCD may result from a functional defect of the Runx2/Cbfβ heterodimeric complex in various cell types. It also indicates that, in terms of the pathogenesis of CCD, Cbfβ deficiency may be equivalent to RUNX2 haploinsufficiency as it relates to the function of the Runx2/Cbfβ complex in skeletogenesis.

Indispensable Role of Hypertrophic Chondrocytes in Endochondral Bone Formation. The role of hypertrophic chondrocytes in endochondral bone formation is a long-standing question. Our results showed that there is a shortened growth plate, a decreased and disorganized proliferative zone, and a reduction in hypertrophic chondrocytes in *Cbfβ*$^{f/f}$*Osx-Cre* mutant mice. However, growth plate development in *Cbfβ*$^{f/f}$*Col1α1-Cre* mutant mice is normal compared with the WT control. These phenotypes of the mutant mice provided a unique opportunity to address the role of hypertrophic chondrocytes in endochondral bone formation. Our results indicate that Cbfβ maintains trabecular bone formation through its function in chondrocytes. Based on the severe endochondral bone defects in *Cbfβ*$^{f/f}$*Osx-Cre* mutant mice (Figs. 1 and 3) and the mild endochondral bone defects in *Cbfβ*$^{f/f}$*Col1α1-Cre* mutant mice (Fig. 4), we conclude that the role of hypertrophic chondrocytes in endochondral bone formation is indispensable.

We hypothesize that the lack of trabecular bone is not the result of a lack of osteoblast precursors and preosteoblasts but may be a result of a lack of the factor(s) (such as Ihh) secreted by prehypertrophic or hypertrophic chondrocytes, although the mechanism of this dependence remains to be identified.

Cbfβ Plays an Indispensable Role in Postnatal Skeletal Development and Homeostasis by Up-Regulating the Expression of *Atf4* and *Osterix*. Cbfβ deficiency reduced the expression of several key factors that mediate osteoblast formation and/or function (e.g., Osx and Atf4). This suggests that Cbfβ may have a role in promoting the commitment of osteoblast precursors into the osteoblast lineage. Yang et al. reported that ATF4 is a critical regulator of osteoblast differentiation and function (15). However, how ATF4 is regulated at the transcriptional regulation level remains unclear. Our study shows that Cbfβ associates with the promoter regions of *Osx* and *Atf4* and highly up-regulates the expression of *Atf4* at the transcriptional regulation level as shown by ChIP assay, microarray analysis, quantitative PCR (qPCR) analysis, and promoter reporter assay. We also found that Cbfβ is crucial for the later stages of chondrocyte differentiation as its deletion affects chondrocyte maturation and the formation of the growth plate.

The Clinical Features of CCD Are Recapitulated in *Cbfβ$^{f/f}$Osx-Cre* Mice. Because Runx2 functions as a heterodimer with CBFβ, it has been suspected that Cbfβ may be responsible for some cases of CCD. Although no CBFβ mutation has yet been identified in classical CCD patients, our *Cbfβ$^{f/f}$Osx-Cre* mouse models support the notion that search genetic alterations in the *CBFβ* gene may be responsible for CCD in those patients with no *RUNX2* mutation. Our results are in agreement with that of previous studies reporting that Runx2 deficiency causes an arrest in tooth development (16) and that Osx is necessary for odontoblast differentiation (13). These findings provide great insight into the pathogenesis of CCD and the role of Cbfβ in both postnatal skeletal and tooth development. The insights resulting from this study may assist in the development of novel treatments for CCD and other bone diseases.

Materials and Methods

Animal Experimentation and Generation of Cbfβ cKO Mice. *Cbfβ$^{f/f}$* mice (Jackson Laboratory, strain name B6.129P2-*Cbfβ^{tm1Itan}/J*) were crossed with skeletal tissue cell (including osteoblast precursors, osteoblasts, chondrocytes, and odontoblasts)-specific *Osx-cre* mice (12) [*Tg(Sp7-tTA,tetO-EGFP/cre)1Amc*, Mouse Genome Informatics] or osteoblast-specific *Col1α1-Cre* mice. Their progeny were crossed with *Cbfβ$^{f/f}$* mice to obtain *Cbfβ$^{f/f}$Col1α1-Cre* mice or *Cbfβ$^{f/f}$Osx-Cre* mice. In our study, we only use one copy of *Osx-Cre* (*Cbfβ$^{f/f}$ Osx-Cre/+*) in the cKO mutation. We used *Cbfβ$^{f/f}$* mice and *Osx-Cre/+* mice as controls. Mouse C57/BL6 WT calvarial cells were also used. All research procedures using mice were approved by the University of Alabama at Birmingham (UAB) Animal Care and Use Committee and conformed to the National Institutes of Health guidelines.

Skeletal Analysis, Tissue Preparation, and Histology Stains. Histomorphometric samples were processed as nondecalcified hard-tissue sections. Bone parameters were quantified via 6 μm sections obtained from 3-wk-old mice. For paraffin sections, samples were decalcified and dehydrated in ethanol, cleared in xylene, embedded in paraffin, and sectioned at 6 μm with Leica microtome and mounted on Superfrost Plus slides (Fisher). Histological analysis was performed including staining with Alcian blue, safranin O, and H&E using paraffin sections.

ChIP and Promoter Analyses. Cells were derived from calvaria of newborn WT mice and mutant mice. *Osx*, *Runx2*, and *Atf4* promoter sequences were analyzed for putative Runx binding sites with PROMO3.0 (http://alggen.lsi.upc.es/) using version 8.3 of the TRANSFAC database. ChIP was performed using monoclonal anti-Cbfβ antibody (sc-20693X) and DNA extraction, and qPCR was performed. The *Osx*, *Runx2*, and *Atf4* promoters were amplified using PCR from BAC clones provided by the BACPAC Resource Center at Children's Hospital Oakland Research Institute. These amplified fragments were cleaved and ligated into the pGL3 vector from Promega. The calvarial cells were cotransfected with each construct with the amount of 100 ng per well as well as pSV–β-galactosidase construct with the amount of 50 ng per well (Promega) and incubated for 6–8 h. The culture medium was replaced with osteogenic medium and cultured for 2 d. Luciferase activity was measured using a Steady-Glo luciferase assay system (Promega cat. no. E2510). pSV–β-galactosidase activity was measured using a β-galactosidase Enzyme Assay system (Promega cat. no. E2000).

Statistical Analysis. All data are presented as the mean ± SD ($n \geqq 6$). Statistical significance was assessed using Student *t* test. *P* values < 0.05 were considered significant. Data are expressed as mean ± SD, $n \geqq 6$, $^{*}P < 0.05$, $^{**}P < 0.01$, $^{***}P < 0.001$. The results are representative of at least four individual experiments. The analyses of the data were performed with the SPSS 16.0 software (SPSS Incorporation).

Please see *SI Materials and Methods* for additional details.

ACKNOWLEDGMENTS. We appreciate the assistance provided by the Center for Metabolic Bone Disease at the University of Alabama at Birmingham (Grant P30 AR046031). We are also grateful for the assistance from the Small Animal Phenotyping Core, Metabolism Core, and Neuroscience Molecular Detection Core Laboratory at the University of Alabama at Birmingham (Grant P30 NS0474666). This work was supported by National Institutes of Health Grants AR-44741 and AR-055307 (both to Y.-P.L.).

1. Otto F, et al. (1997) Cbfa1, a candidate gene for cleidocranial dysplasia syndrome, is essential for osteoblast differentiation and bone development. *Cell* 89(5):765–771.
2. Mundlos S, et al. (1997) Mutations involving the transcription factor CBFA1 cause cleidocranial dysplasia. *Cell* 89(5):773–779.
3. Lee B, et al. (1997) Missense mutations abolishing DNA binding of the osteoblast-specific transcription factor OSF2/CBFA1 in cleidocranial dysplasia. *Nat Genet* 16(3):307–310.
4. Goto T, et al. (2004) Large fontanelles are a shared feature of haploinsufficiency of RUNX2 and its co-activator CBFB. *Congenit Anom (Kyoto)* 44(4):225–229.
5. Khan A, Hyde RK, Dutra A, Mohide P, Liu P (2006) Core binding factor beta (CBFB) haploinsufficiency due to an interstitial deletion at 16q21q22 resulting in delayed cranial ossification, cleft palate, congenital heart anomalies, and feeding difficulties but favorable outcome. *Am J Med Genet A* 140(21):2349–2354.
6. Kanatani N, et al. (2006) Cbf beta regulates Runx2 function isoform-dependently in postnatal bone development. *Dev Biol* 296(1):48–61.
7. Sasaki K, et al. (1996) Absence of fetal liver hematopoiesis in mice deficient in transcriptional coactivator core binding factor beta. *Proc Natl Acad Sci USA* 93(22):12359–12363.
8. Komori T, et al. (1997) Targeted disruption of Cbfa1 results in a complete lack of bone formation owing to maturational arrest of osteoblasts. *Cell* 89(5):755–764.
9. Yoshida CA, et al. (2002) Core-binding factor beta interacts with Runx2 and is required for skeletal development. *Nat Genet* 32(4):633–638.
10. Kundu M, et al. (2002) Cbfbeta interacts with Runx2 and has a critical role in bone development. *Nat Genet* 32(4):639–644.
11. Miller J, et al. (2002) The core-binding factor beta subunit is required for bone formation and hematopoietic maturation. *Nat Genet* 32(4):645–649.
12. Rodda SJ, McMahon AP (2006) Distinct roles for Hedgehog and canonical Wnt signaling in specification, differentiation and maintenance of osteoblast progenitors. *Development* 133(16):3231–3244.
13. Chen S, et al. (2009) Runx2, osx, and dspp in tooth development. *J Dent Res* 88(10):904–909.
14. Dacquin R, Starbuck M, Schinke T, Karsenty G (2002) Mouse alpha1(I)-collagen promoter is the best known promoter to drive efficient Cre recombinase expression in osteoblast. *Dev Dyn* 224(2):245–251.
15. Yang X, et al. (2004) ATF4 is a substrate of RSK2 and an essential regulator of osteoblast biology; implication for Coffin-Lowry Syndrome. *Cell* 117(3):387–398.
16. D'Souza RN, et al. (1999) Cbfa1 is required for epithelial-mesenchymal interactions regulating tooth development in mice. *Development* 126(13):2911–2920.

Supporting Information

Chen et al. 10.1073/pnas.1310617111

SI Materials and Methods

Cbfβ$^{f/f}$Osx$^{Cre/+}$ Generation. We only use one copy of *Osx-Cre* (*Cbfβ$^{f/f}$ Osx$^{Cre/+}$*) in the conditional knockout (cKO) mutation phenotype analysis. *Cbfβ$^{f/f}$Osx$^{Cre/+}$* mice were generated by crossing *Cbfβ$^{f/f}$* mice and *Cbfβ$^{f/+}$* mice with *Osx$^{Cre/+}$* mice and *Cbfβ$^{f/f}$* mice as the control. We did not find any delayed cortical bone growth or any other skeletal defect in the control mice.

Radiographic Procedures. For X-ray analysis, radiography was performed using the Faxitron Model MX-20 at 26 kV by the University of Alabama at Birmingham (UAB) Small Animal Bone Phenotyping Core associated with the Center for Metabolic Bone Disease. The microcomputed tomography analysis was performed to determine the bone mass of fixed femurs by the UAB Small Animal Bone Phenotyping Core associated with the Center for Metabolic Bone Disease.

Histomorphometric Analysis. Histomorphometric samples were processed as nondecalcified hard-tissue sections as described (1). Bone parameters were quantified via 6 μm sections obtained from 3-wk-old mice.

Skeletal Analysis. For skeletal preparations, mice were skinned, eviscerated, fixed in 95% (vol/vol) ethanol, cleared in acetone, stained with Alizarin red and/or Alcian blue stains, and sequentially cleared in 1% KOH. Cartilage and mineralized bone were characterized by different colors (blue and red, respectively) after the stain, according to standard protocols (2).

Tissue Preparation and Histology Stains. Femurs and tibiae of mice were harvested, skinned, and fixed in 4% (wt/vol) paraformaldehyde overnight. Samples were then dehydrated in ethanol solution and decalcified in 10% (wt/vol) EDTA for 1–4 wk. For paraffin sections, samples were dehydrated in ethanol, cleared in xylene, embedded in paraffin, and sectioned at 6 μm with Leica microtome and mounted on Superfrost Plus slides (Fisher).

For frozen sections, samples were infiltrated in 30% (wt/vol) sucrose, embedded in optimal cutting temperature compound, sectioned at 8 μm with a freezing microtome, and affixed to Superfrost Plus Gold slides (Fisher). Histological analysis was performed including staining with Alcian blue, safranin O, hematoxylin/eosin (H&E) (3), and Goldner's trichrome stains (4) using paraffin sections.

TRAP Staining. Parraffin sections were stained using the Acid Phosphatase, Leukocyte [tartrate-resistant acid phosphatase (TRAP)] Kit (387A-1KT, Sigma) following the manufacturer's instructions, counterstained with hematoxylin, dehydrated, and mounted. Data are included as graphs of osteoclasts per millimeter of bone perimeter.

Von Kossa Staining. Von Kossa staining was performed as follows. Cells were washed with Ca^{2+}/Mg^{2+}–free PBS and then fixed on slides in 10% (vol/vol) cold Neutral Formalin solution. We then added 2.5% (wt/vol) silver nitrate solution, and the slides were incubated under UV light for 5–10 min. After incubation, the unincorporated silver nitrate was removed by washing with 5% (wt/vol) sodium thiosulfate.

Proliferation Assay. To detect proliferating cells in culture, immunochemistry staining was performed according to the manufacturer's instructions. Horseradish peroxidase-conjugated proliferating cell nuclear antigen (PCNA) antibodies (cat. no. 93–1143; Zymed Laboratories Inc.) and Vector DAB substrate (3,3′-diaminobenzidine) kits (cat. no. SK-4100; Vector Laboratories) were used.

Immunohistochemistry. For immunohistochemistry, samples were embedded in paraffin and sectioned as described previously. The Vector DAB substrate kit (cat. no. SK-4100; Vector Laboratories) was used along with secondary staining kits for mouse (on mouse) and rabbit (cat. no. BMK-2202 and PK-6101, respectively; Vector Laboratories) and primary antibodies for Osterix (ab22552; Abcam), Runt-related transcription factor 2 (RUNX2) (ab23981; Abcam), and Cbfβ (sc-56751; Santa Cruz).

Immunofluorescence. Samples were embedded in tissue freezing medium, and sections were cut at a thickness of 8 μm with a cryotome. Pictures were taken by Leica confocal microscopes (SP1) and a Zeiss fluorescent microscope (Zeiss Axio Imager). The following antibodies were used: rabbit anti-Col10 (1:200; ab58632, Abcam), anti-Runx1 (ab35962, Abcam), Runx2 (pc-287, Merck/Millipore), and Runx3 (sc-30197, Santa Cruz).

Primary Cell Culture. Calvarial cells were isolated from newborn mice and seeded in cell culture dishes at a density of 3×10^3 cells/cm^2 as previously described (5). After growing to confluence, cells were induced to differentiate into osteoblasts using osteogenic medium and BGJb medium (Gibco, 12591) supplemented with 10% (vol/vol) FBS, 50 μg/mL L-ascorbic acid (Sigma, A4544), and 5 mM β-glycerolphosphate (Sigma, G9891). Osteoblastogenesis was analyzed by alkaline phosphatase (ALP) staining according to the manufacturer's manual (sigma, A2356) on day 14. Osteoblast mineralization was examined by Von Kossa staining on day 21.

GeneChip Analysis. We analyzed independently prepared duplicate samples containing primary osteoblasts derived from the calvarial bone of C57/BL6 wild-type (WT) mice as previously described (3). TRIzol reagent (Life Technologies) was used according to the manufacturer's protocol to extract total RNA from C57/BL6 WT calvarial cells after culturing for 7 or 21 d. RNA profiling was performed by using the Affymetrix mouse 430 Plus 2.0 array as described (6). Replicate samples were averaged for reporting.

Promoter Analyses. To determine 5′-flanking regulatory activity, calvarial cells were cultured for 5 d in osteogenic medium, reseeded on 96-well plates, and transfected with constructs (Fig. S8) using Fugene6 reagent (Roche) as described (4). The calvarial cells were cotransfected with each construct (Fig. S8) with the amount of 100 ng per well as well as pSV–β-galactosidase construct (Promega) (50 ng/well) and incubated for 3 h as described (4, 7). The culture medium was replaced with osteogenic medium and cultured for 2 d. Luciferase activity was measured using a Steady-Glo luciferase assay system (Promega). PGL3 basic reporter vectors were used as controls (Promega). Luminescence was detected with a luminometer (BioTek Synergy 2). The luciferase activity in transfected cultures was standardized by normalization to β-galactosidase activity, and the protein concentration of cell extracts was determined using a protein assay kit (BioRad) as described (4, 7). In all experiments, constructs are tested in triplicate.

Quantitative Real-Time PCR Analysis. mRNA was extracted from cultured cells on days 7, 14, and 21 using TRIzol (Invitrogen) and then reverse-transcribed into cDNA according to the manu-

facturer's manual (qScript cDNA Synthesis Kit, Quanta Biosciences Inc.). Expressions of osteoblastic marker genes were analyzed by quantitative real-time PCR (qRT-PCR) using the StepOne Real-Time PCR System (Life Technologies). Expression of Atf4, Col1α1, Spp1, Runx2, Sox9, OPG, RANKL, and OCN was analyzed. The primer sequences are available upon request.

Western Blot Analyses. Protein samples extracted from calvaria-derived osteoblasts were prepared in protein lysis buffer, resolved on SDS/PAGE, and electrotransferred onto nitrocellulose membranes. Immunoblotting was performed according to the manufacturer's instructions. Osteoblast- and chondrocyte-related regulators and marker genes including Cbfβ, Runx2, Col1α1, Osterix, ATF4, and Sox9 were detected using primary antibodies as follows: rabbit anti-Cbfβ (1:1,000; ab72696, Abcam), rabbit anti-Runx2 (1:2,000; ab23981, Abcam), rabbit anti-Col1α1 (1:1,000; ab34710, Abcam), rabbit anti-Sp7/Osterix (1:1,000; ab22552, Abcam), mouse anti-ATF4 (1:1,000; ab50546, Abcam), rabbit anti-sox9 (H-90) (1:1,000; sc-20095, Santa Cruz Biotechnology), and mouse anti–β-tubulin (1:100, cell lysates). Horseradish peroxidase-linked anti-rabbit IgG and horseradish peroxidase-linked anti-mouse IgG were purchased from Cell Signaling (nos. 7074 and 7076).

Chromatin Immunoprecipitation. Cells were derived from calvaria of newborn WT mice and mutant mice as described (8). *Osx*, *Runx2*, and *Atf4* promoter sequences were analyzed for putative Runx binding sites with PROMO3.0 (http://alggen.lsi.upc.es/) using version 8.3 of the TRANSFAC database. Chromatin immunoprecipitation (ChIP) was performed as described (4). After immunoprecipitation using monoclonal anti-Cbfβ antibody (sc-20693X) and DNA extraction, quantitative PCR was performed using the following primers in the promoter region of the mouse gene *Osx*, *Runx2*, and *Atf4*. The primer sequences were as follows: Osx 1a (forward 5′-ATTTATACTCCGTCCCCGCC-3′, reverse 5′-AGCTGCAAAAGTGACCCG-3′), Osx 2b (forward 5′-AGATCGTCCTGTCTCTGCCT-3′, reverse 5′-CAGCCTGGTCTACATGGCAA-3′), Osx 3b (forward 5′-GGACTGGCTGAGAACAGAGG-3′, reverse 5′-GAAGTCTGGGGAGGACGACT-3′), Osx 4b (forward 5′-CCACAGCAAGCTTTTCCCAC-3′, reverse 5′-GGATGATGTGCCAAGTGTGC-3′), Runx2 1a (forward 5′-TGACCACATCTTAGGTCACA-3′, reverse 5′-ACTGATACGTTCTGTTTACATTTCAC-3′), Runx2 2b (forward 5′-TGAGAGGCAGGAGGATCACA-3′, reverse 5′-ACCCTTGGCTTATGTCCTATTTGT-3′), Runx2 3b (forward 5′-TCATGGGTGGTTGGGGTAGA-3′, reverse 5′-TTACCCACTTCCTGGTCTGC-3′), Runx2 4a (forward 5′-TGGAAGCACAGCATATCAATCAA-3′, reverse 5′-GGTTGAGATTCCAGGCCCTT-3′), Atf4 1b (forward 5′-TTCCTTATGGCTGTCAGCGG-3′, reverse 5′-AAGCAAGGCCACCTTCTACC-3′), Atf4 2a (forward 5′-CGTCTTCTGCAGCATGGGAA-3′, reverse 5′-CCCGTCGTATTCCTAGCACC-3′), and Atf4 3a (forward 5′-GCTGGAGTTGGAAAGAGCCT-3′, reverse 5′-AGGTACTGGTCAAGGCCTCA-3′).

1. Kiviranta R, et al. (2005) Impaired bone resorption in cathepsin K-deficient mice is partially compensated for by enhanced osteoclastogenesis and increased expression of other proteases via an increased RANKL/OPG ratio. *Bone* 36(1):159–172.
2. McLeod MJ (1980) Differential staining of cartilage and bone in whole mouse fetuses by alcian blue and alizarin red S. *Teratology* 22(3):299–301.
3. Feng S, et al. (2013) Silencing of atp6v1c1 prevents breast cancer growth and bone metastasis. *Int J Biol Sci* 9(8):853–862.
4. Chen W, et al. (2013) C/EBPα regulates osteoclast lineage commitment. *Proc Natl Acad Sci USA* 110(18):7294–7299.
5. Logan M, et al. (2002) Expression of Cre recombinase in the developing mouse limb bud driven by a Prxl enhancer. *Genesis* 33(2):77–80.
6. Yang S, Li YP (2007) RGS10-null mutation impairs osteoclast differentiation resulting from the loss of [Ca2+]i oscillation regulation. *Genes Dev* 21(14):1803–1816.
7. Kamolmatyakul S, et al. (2004) IL-1alpha stimulates cathepsin K expression in osteoclasts via the tyrosine kinase-NF-kappaB pathway. *J Dent Res* 83(10):791–796.
8. Gosset M, Berenbaum F, Thirion S, Jacques C (2008) Primary culture and phenotyping of murine chondrocytes. *Nat Protoc* 3(8):1253–1260.

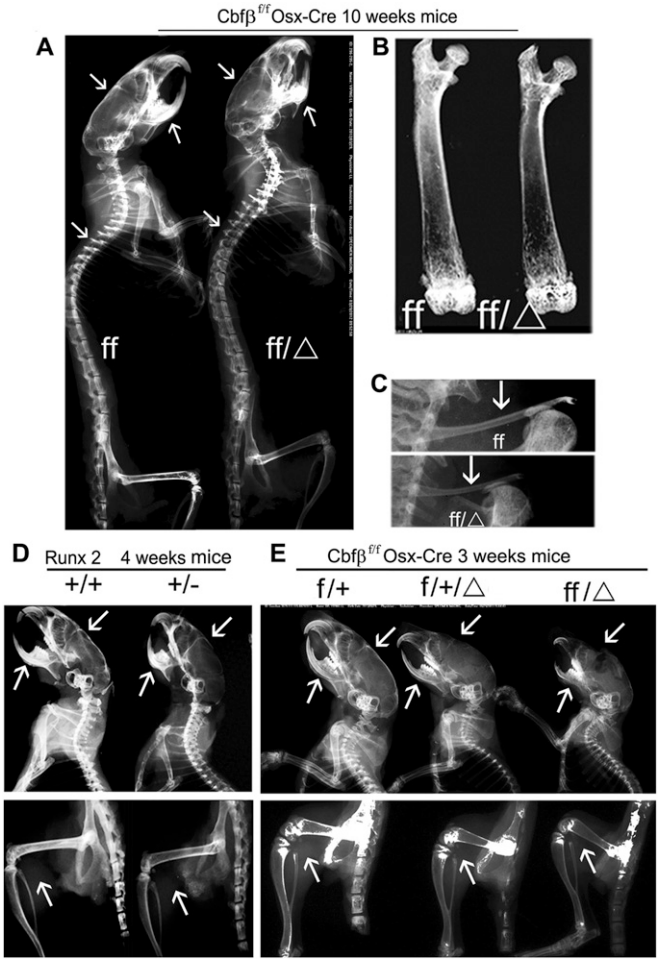

Fig. S1. Adult *Cbfβ*$^{f/f}$ and *Cbfβ*$^{f/+}$ *Osx-Cre* mice have decreased bone mineralization similar to *Runx2*$^{+/-}$ mice and severely defective clavicles. (*A*–*C*) X-ray analysis of the whole body (*A*), femurs (*B*), and clavicles (*C*) of 10-wk-old *Cbfβ*$^{f/f}$ *Osx-Cre* (ff/Δ) and WT (ff) mice. Data showed severe defects in bone mineralization and skeletal development in the mutant mice compared with their WT littermates. Also, the clavicles of the mutant mice were drastically shorter. Arrows in *A* show that the calvaria and vertebral column were less calcified in the mutant mice compared with WT mice. Arrows in *C* show hypoplastic/aplastic clavicles in the mutant mice compared with WT mice. (*D*) X-ray analysis of 4-wk-old Runx2-heterozygous mutant ($^{+/-}$) and WT ($^{+/+}$) mice. There was decreased bone mineralization in the mutant mice compared with their WT cohorts. Arrows show that the calvaria and femurs were less calcified in the mutant mice and the mandibles were underdeveloped in the mutant mice. (*E*) X-ray analysis of 3-wk-old *Cbfβ*$^{f/+}$(f/+), *Cbfβ*$^{f/+}$ *Osx-Cre* (f/+/Δ), and *Cbfβ*$^{f/f}$ *Osx-Cre* (ff/Δ). There was a milder cleidocranial dysplasia (CCD) phenotype in *Cbfβ*$^{f/+}$ *Osx-Cre* mice and a more severe CCD phenotype in *Cbfβ*$^{f/f}$ *Osx-Cre* mice.

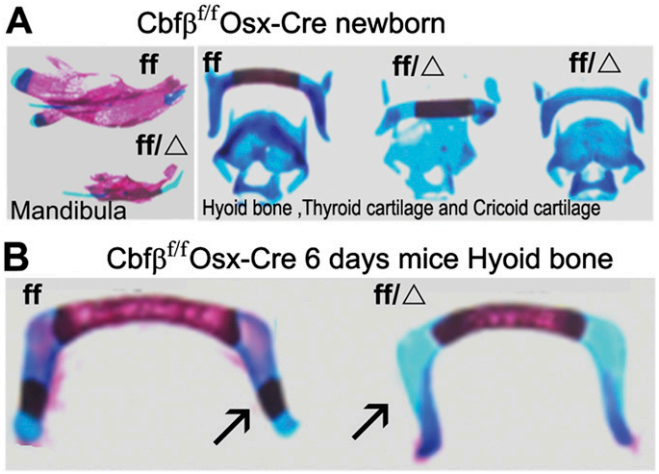

Fig. S2. *Cbfβ$^{f/f}$Osx-Cre* mice have undercalcified mandibula, hyoid bones, and thyroid cartilage. (*A*) Mandibula, hyoid bone, thyroid cartilage, and cricoid cartilage of *Cbfβ$^{f/f}$ Osx-Cre* (ff/Δ) and WT (ff) mice were stained by Alizarin red and Alcian blue staining at the newborn stage. (*B*) The hyoid bone of *Cbfβ$^{f/f}$ Osx-Cre* and WT mice were stained by Alizarin red and Alcian blue staining at 6 d of age. Arrows show decreased mineralization of the hyoid bone in the mutant mice compared with WT mice. *Cbfβ$^{f/f}$ Osx-Cre* mice had shorter mandibula and hyoid bones. Furthermore, the hyoid bone and thyroid cartilage of the mutant mice had reduced mineralization. These findings indicate that ablation of Cbfβ in the osteoblast precursors leads to defective postnatal bone development.

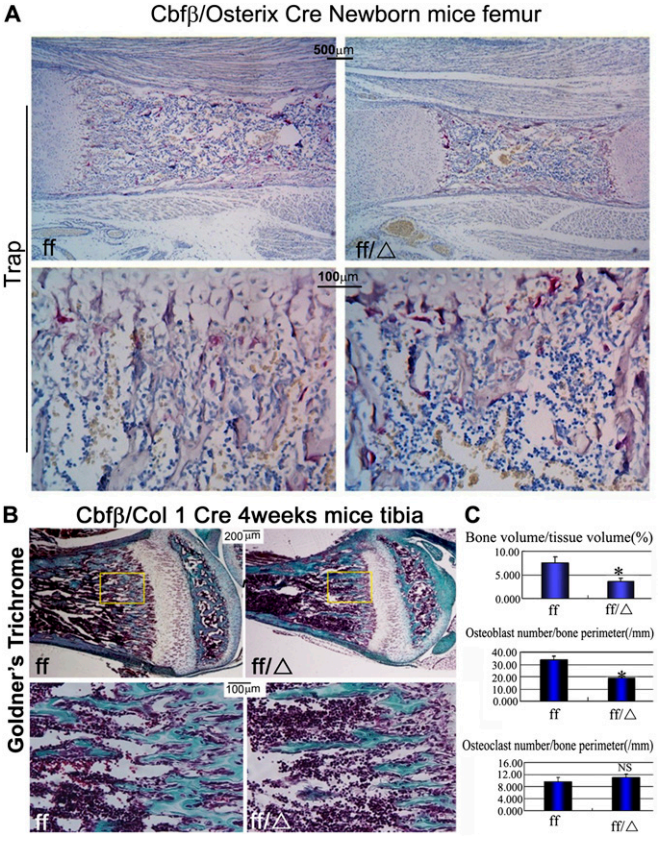

Fig. S3. TRAP staining of *Cbfβ$^{f/f}$ Osx-Cre*. (*A*)TRAP stain of femur plastic sections of newborn *Cbfβ$^{f/f}$ Osx-Cre* and WT (ff) mice. Osteoclast number is similar between WT and mutant mice. (*B*) Goldner's Trichrome staining of tibial plastic sections of 4-wk-old *Cbfβ$^{f/f}$ Col1α1-Cre* (*ff/Δ*) and WT (ff) mice. For histological detail of trabeculae, the bottom row shows a higher magnification (yellow boxes). (*C*) Histomorphometric analysis and quantification of the data shown in *A*. *Cbfβ$^{f/f}$ Col1α1*-cre mice had a significant reduction in trabecular bone and osteoblast numbers but not in osteoclast numbers. Data are expressed as mean ± SD, $n \geqq 6$, $^*P < 0.05$.

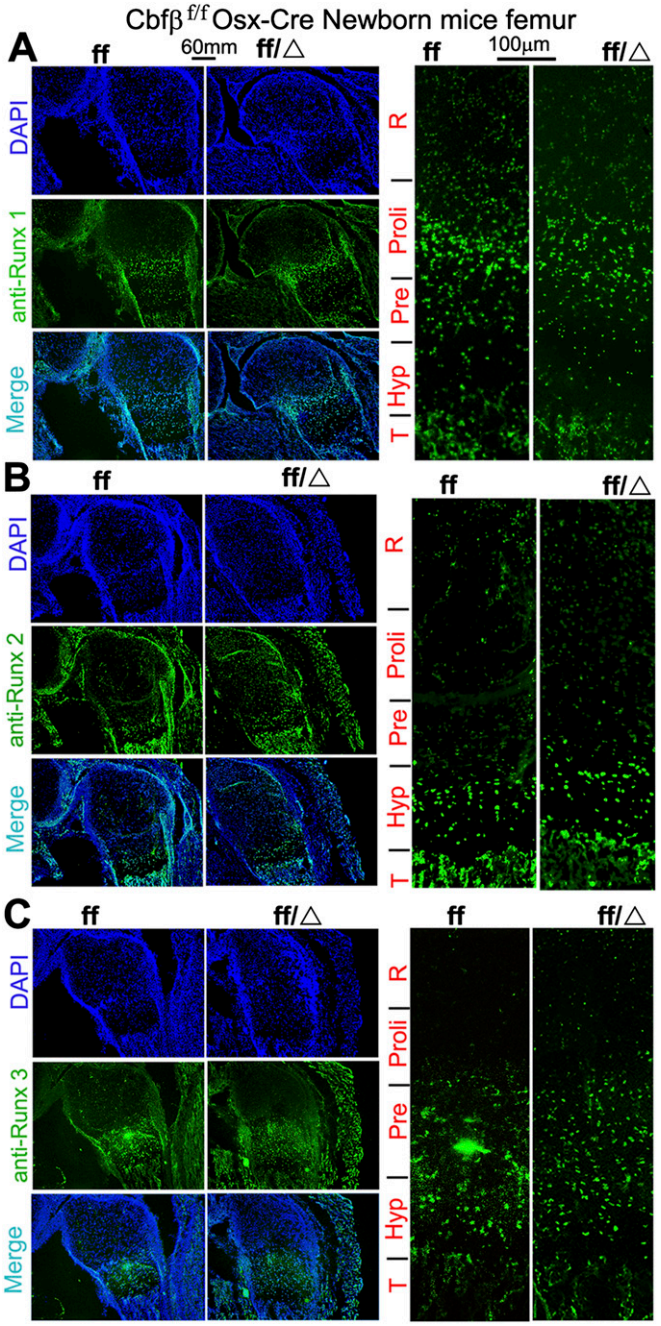

Fig. S4. Expression of Runx1, Runx2, and Runx3 is unchanged in chondrocytes of *Cbfβ*$^{f/f}$ *Osx-Cre* mice relative to WT mice. (*A*–*C*) Immunofluorescent staining for Runx1 (*A*), Runx2 (*B*), and Runx3 (*C*) on frozen sections of femur growth plates from newborn *Cbfβ*$^{f/f}$ *Osx-Cre* and WT mice. Bright field views were copresented. Hyp, hypertrophic zone; Pre, prehypertrophic zone; Proli, proliferating zone; R, resting zone; T, trabecular bone.

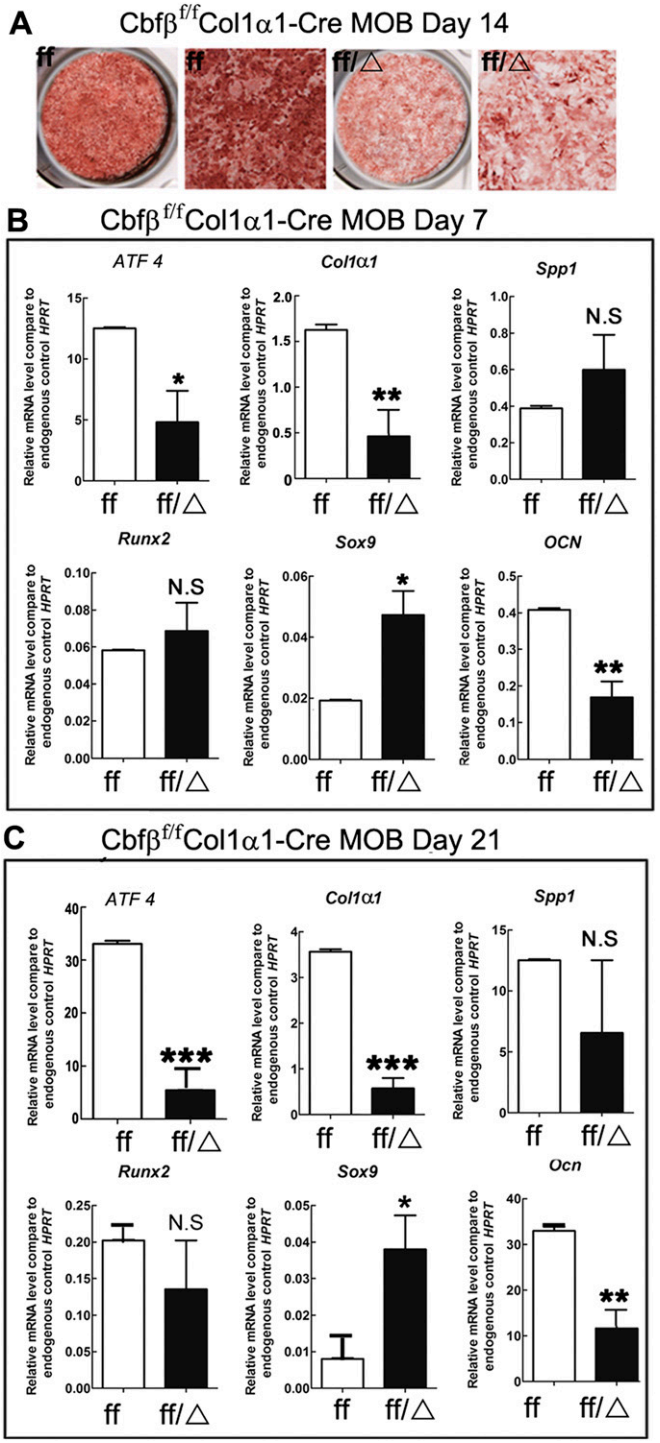

Fig. S5. Primary calvarial cells cultured from *Cbfβ*$^{f/f}$ *Col1α1-cre* mice have impaired osteoblastogenesis. (*A*) Calvarial cells from WT (ff) or *Cbfβ*$^{f/f}$ *Col1α1-cre* (ff/Δ) newborn mice were submitted to osteoblastogenesis assays. Osteoblastogenesis was analyzed by ALP activity on day 14. (*B* and *C*) mRNA expression levels of Atf4, Col1α1, Spp1, Runx2, Sox9, and OCN were determined by qRT-PCR after culture in osteoblast differentiation media for 7 d (*B*) or 21 d (*C*). The results demonstrate that deletion of Cbfβ affects osteoblastogenesis in part by affecting the expression of osteoblast and chondrocyte genes. Data are normalized to the housekeeping gene, *hypoxanthine-guanine phosphoribosyl transferase*. Results are expressed as mean ± SD, $n \geqq 6$ in each group. $^{*}P < 0.05$, $^{**}P < 0.01$.

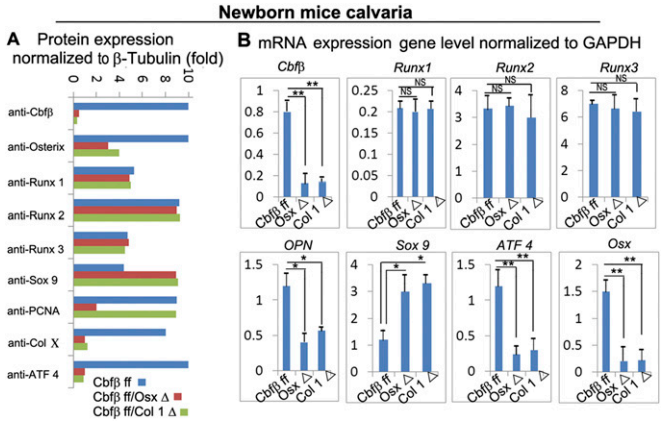

Fig. S6. Expression of osteoblast-related genes in calvarial cells in osteoblastogenic media conditions is attenuated in *Cbfβ*$^{f/f}$ *Osx-Cre*– and *Cbfβ*$^{f/f}$ *Col1α1-Cre*–derived cells relative to WT. (*A*) Quantification of protein expression, from Western blot (Fig. 7*D*), normalized to β-tubulin from the calvaria of *Cbfβ*$^{f/f}$ *Osx-Cre*, *Cbfβ*$^{f/f}$ *Col1α1-Cre*, and WT mice. (*B*) mRNA expression levels of *Cbfβ*, *Runx1*, *Runx2*, *Runx3*, *Opn*, *Sox9*, *Atf4*, and *Osx* in calvarial cells from *Cbfβ*$^{f/f}$ *Osx-Cre*, *Cbfβ*$^{f/f}$ *Col1α1-Cre*, and WT mice were determined by qRT-PCR after culturing in the osteoblast differentiation media for 14 d. Data were normalized to *Gapdh*. Results are expressed as means ± SD, $n \geq 6$ in each group. $^{*}P < 0.05$, $^{**}P < 0.001$.

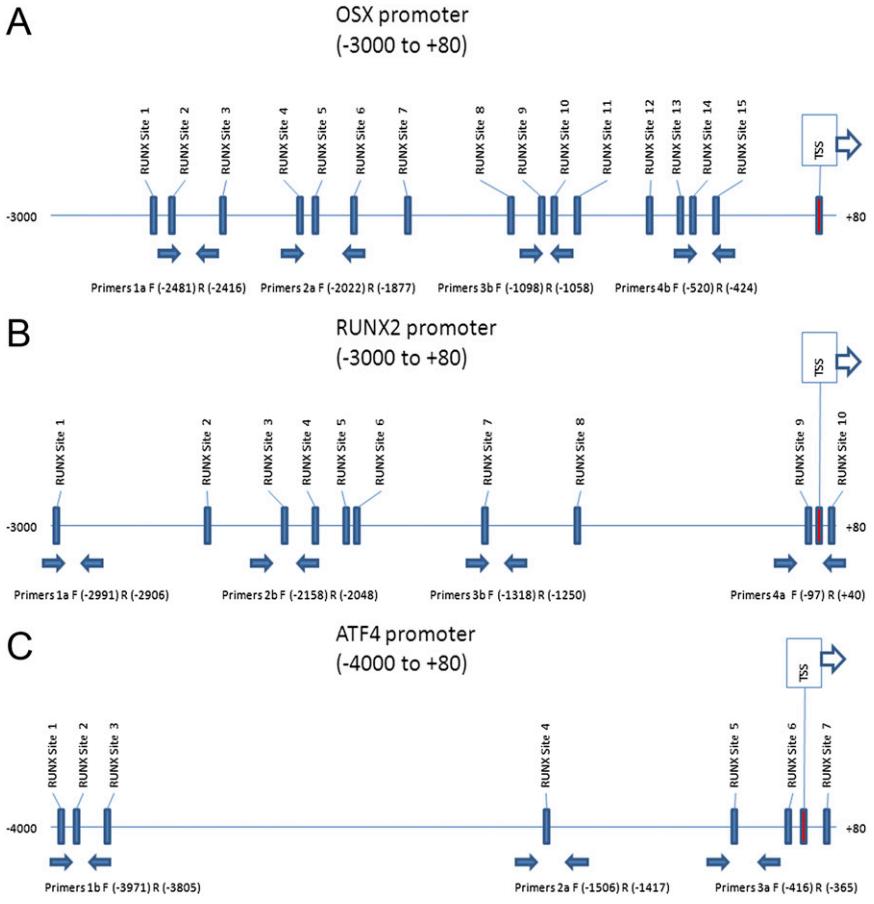

Fig. S7. *Osx*, *Runx2*, and *Atf4* have predicted Runx/Cbf binding sites. Schematic display of *Osx* (–3000/+80) (*A*), *Runx2* (–3000/+80) (*B*), and *Atf4* (–4000/+80) (*C*) promoter regions. TSS (transcriptional start site), predicted Runx-binding sites, and ChIP primer positions (F, forward; R, reverse) are indicated in the figure.

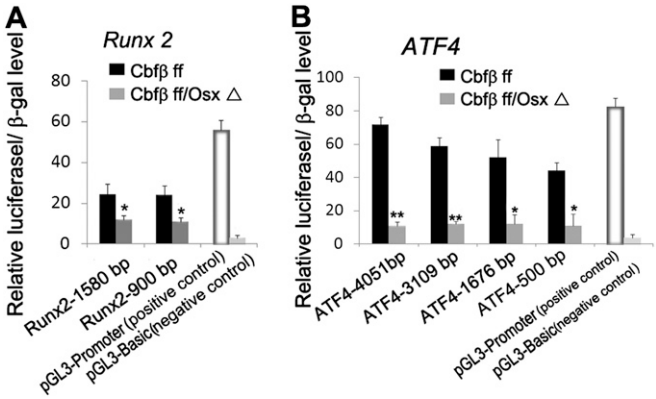

Fig. S8. Expression driven by the *Runx2* and *Atf4* promoters is diminished in *Cbfβ*$^{f/f}$ *Osx-Cre* chondrocytes. (*A*) *Runx2* promoter fragments were inserted into the pGL3–basic vector. Calvarial cells were transfected with pGL3–control, pGL3–*Runx2*–1,580 bp, or pGL3–*Runx2*–900 bp. Luciferase was detected 48 h posttransfection. The signal was normalized to β-gal activity. (*B*) *Atf4* promoter fragments were inserted into the pGL3–basic vector. Calvarial cells were transfected with pGL3–control, pGL3–*Atf4*–4,051 bp, pGL3–*Atf4*–3,109 bp, pGL3–*ATF4*–1,676 bp, or pGL3–*ATF4*–500 bp. β-gal expression plasmids were co-transfected as control. Luciferase was detected 48 h posttransfection. The signal was normalized to β-gal activity. Results are presented as mean ± SD, $n \geqq 6$ in each group. $^{*}P < 0.05$, $^{**}P < 0.01$, $^{***}P < 0.005$.